2019 International Conference on Internet of Things (iThings) and IEEE Green Computing and Communications (GreenCom) and IEEE Cyber, Physical and Social Computing (CPSCom) and IEEE Smart Data (SmartData)

Maximizing Energy Harvesting with Adjustable Solar Panel for BLE Beacon

Perm Soonsawad, Kang Eun Jeon, James She, Ching Hong Lam and Pai Chet Ng
HKUST-NIE Social Media Lab, Hong Kong University of Science and Technology
Email: {psoonsawad, kejeon, eejames, chlamaq and pcng}@ust.hk

***Abstract*—Bluetooth Low Energy (BLE) beacons can be powered up with a small coin cell battery. The problem with battery-powered beacon is that frequent battery replacement is required. Such a battery replacement process can be very tedious considering the massive amount of already deployed beacons. While solar-powered beacons have emerged as an alternative to the battery-powered beacon, beacon deployment is challenging considering the very low ambient light energy available in indoor environments. This paper presents an innovate solar-powered beacon with an adjustable solar panel. In particular, we employ Markov Decision Process (MDP) to model the angle adjusting problem. The contribution of this paper is two-fold: 1) the MDP formulation is based on the insight obtained from a series of preliminary experiments which unveil the relationship between the incident angle and the harvested power; 2) our experiment shows that the legacy Policy Iteration (PI) and Value Iteration (VI) algorithms achieve similar optimized decision-making by adjusting the angle of solar panels such that to quickly charge up the beacon when it is low in energy. This rapid charging time guarantees the sustainable operation of solar-powered beacons in indoor environments.**

***Index Terms*—energy harvesting; adjustable solar panel; BLE beacon; Markov Decision Process (MDP)**

I. Introduction

The key enabling features of Bluetooth Low Energy (BLE) beacons in empowering the Internet of Things (IoT) have attracted a lot of interest recently [1] [2], and many BLE beacons have been deployed in indoor environments to promote IoT applications. For example, proximity-based marketing [3], proximity-based interaction [4], indoor localization [5], distance estimation [6] and proximity detection [7], etc. Most of these beacons are powered by batteries, with frequent battery replacement is required to ensure the continual operation of the beacons. Such battery replacement can be labor intensive and can increase management cost considering the massive number of deployed beacons inside a building. Consequently, reducing the scalability of BLE beacon-based infrastructure. Recently, solar-powered beacons (e.g., HKUST's luXbeacon X4[1]) has emerged as an alternative solution to the battery-powered beacon [8]. Fig. 1 illustrates these two types of beacon: (a) battery-powered beacon and (b) solar-powered beacon.

While we can deploy the battery-powered beacons at any desired locations, this might not be the case with solar-powered beacons. More precisely, it is important to consider deployment such that a beacon can harvest sufficient energy for its daily operation at the same time as providing its IoT service to users. In contrast to large-scale solar panels deployed in outdoor environments to supply electrical power to the grid, the solar panel used by a typical beacon is very small, even smaller than the solar panel used by mobile power bank. Hence, it is of critical importance to find a suitable deployment location for a solar-powered beacon such that it can harvest sufficient energy for continual operation. For example, a location that has proven to be a good spot for a typical battery-powered beacon in delivering IoT service might not be a good spot for a solar-powered beacon because the spot may have low ambient light energy. Such the issue can be solved by slightly tuning the angle of the deployed beacon.

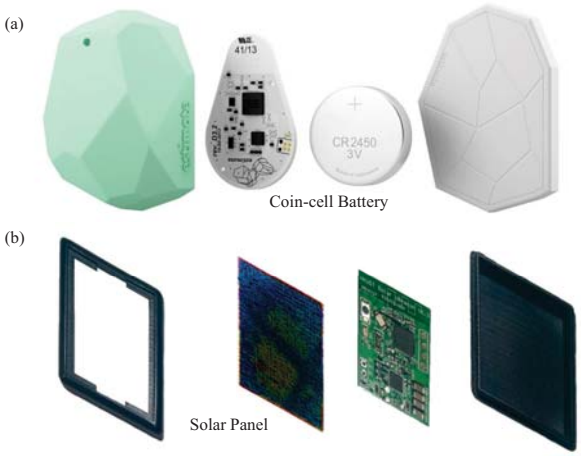

Fig. 1: There are two common types of beacon in the market: (a) battery-powered beacon, and (b) solar-powered beacon.

To allow our solar-powered beacon with adjustable angle to make an optimal decision to achieve fast charging time, this paper employs a Markov Decision Process (MDP) framework to model the angle adjustment problem. Even though a number of prior works have employed MDP for the solar tracking problem with large-scale solar panels installed in outdoor environments [9], [10], most of them exploit the power gain as the reward function. None of the work considers the charging time required to power up a low power device, and how to achieve a fast charging time given the ambient information.

[1]"HKUST luXbeacon X4: An Open Design Initiatives for Greeen, Sustainable and High-Performance IoT"

978-1-7281-2980-8/19/$31.00 ©2019 IEEE
DOI 10.1109/iThings/GreenCom/CPSCom/SmartData.2019.00058

Motivated by deployment challenges, this work provides adjustable angle modeling based on an MDP framework for small-sized solar panels in indoor environments. A series of preliminary experiments are conducted to unveil the factor of *the light's incident angle* θ (one major irradiance component) on the power harvested by the small-scale solar panel. The preliminary analysis provides us a complete prior knowledge in formulating the MDP problem. The contributions of this work is two-fold: 1) the MDP formulation is based on the insight obtained through a series of empirical analysis, which inspires us in designing the reward function based on the power gain to decide the tilting angle of the solar panel with respect to the light source; 2) an analysis of charging time with different supercapacitors is provided before employing the charging time to benchmark the performance of our solar-powered beacon with an adjustable angle. Lastly, simulation results based on the dynamic programming methods: value iteration (VI) and policy iteration (PI), verify the performance of our proposed solution.

The rest of the paper is organized as follows. Section II provides background and preliminary analysis. Section III models the beacon deployment problem. Section IV presents experiments and results related to the modelling, and Section V concludes the paper and presents future work.

II. Background and Preliminarly Analysis

In this section, we describe the light irradiance in the environment before proceeding with preliminary analysis in the next section.

A. Light Irradiance in Indoor Environments

Irradiance is a measurement of the radiant power (emitted by a light source) hitting unit area surface. Hence, it is always measured in watts per square metre (W/m^2). According to [11] and [12], the total power that can be harvested by a solar panel at any instantaneous time is dependent on the irradiance. In this paper, we define the total irradiance hitting R_H on an arbitrarily oriented solar panel mounted on top of a BLE beacon based on the well-developed model by [13]. Specifically, R_H is approximated by summing the following irradiance components:

1) *direct irradiance* R_B: the beam of the light;
2) *diffuse irradiance* R_D: light from the environment;
3) *reflective irradiance* R_R: light reflected from the surroundings.

All three irradiance factors are regulated by the related angles $\alpha, \beta \in [0, 180]^\circ$. Hence, the total irradiance hitting R_H can be expressed as follows:

$$\begin{aligned} R_H(\alpha,\beta) &= \sin(\alpha) R_B^{max} \\ &+ \frac{(1+\cos(\beta))}{2} R_D^{max} \\ &+ (1-\cos(\beta)) R_R^{max}, \end{aligned} \tag{1}$$

where α is the angle between the light beam and the surface of the solar panel, and β is the inclination angle of the surface with respect to the horizontal plane. Fig. 2 illustrates

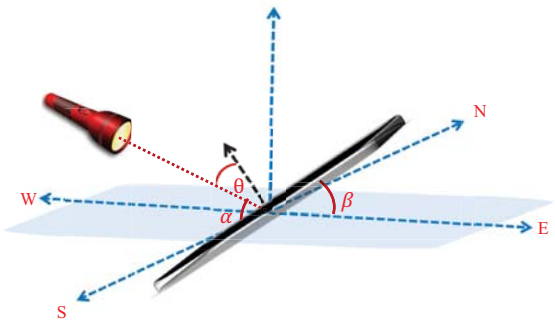

Fig. 2: The angle α and inclination angle β with respect to the solar panel and the horizontal surface.

inclination angles α and β with respect to the surface of a solar panel and θ is the angle between the light beam and the normal.

Note that the first term is based on the cosine effect between the normal angle and the direction to the light source to the solar panel, i.e., $90^\circ - \alpha$, as illustrated in Fig. 2. R_B^{max} is the maximum beam irradiance at which the solar panel is oriented perpendicularly towards the light source, i.e., $90^\circ - \alpha = 0^\circ$. The second term (i.e., the diffuse irradiance component) is derived based on [14], which assumes that every point in an environment diffuses equal radiation on the solar panel's surface. The third term (i.e., the reflective irradiance component), on the other hand, is based on [15], which states that the light is reflected uniformly in all directions. The maximum reflected irradiance R_R^{max} is obtained when the inclination angle of the solar panel is at $\beta = 90^\circ$.

In the following subsections, we provide a preliminary analysis to study the implications of the orientation of the solar panel. Section II-B first presents the measurement setup before discussing the implications in Section II-C.

B. Measurement Setup

Fig. 3(a) illustrates our measurement setup, which consists of a solar panel connected to a multimeter. We mounted the solar panel on a box with a handle, which allow us to rotate the solar panel to any angle. For example, we could rotate the solar panel to 30° as shown in Fig. 3(b). According to the schematic diagram in Fig. 3(b), we define the rotation of the solar panel towards the light source with incident angle θ. In particular, θ indicates the angle between the surface of the solar panel with the normal angle projected by the light source. Let α denote the angle between the light beam and the surface of the solar panel. Then, we have incident angle $\theta = 90^\circ - \alpha$. In the experiment, used an Amorphous solar panel from Panasonic-Sanyo with the dimensions $48.6mm \times 58.1mm (2823.66mm^2)$. A multimeter was used to measure the open-circuit voltage V_{oc} and short-circuit current I_{sc}. The measurement was conducted in a dark room. The same experimental steps were repeated for $\theta = \{0^\circ, \pm 30^\circ, \pm 60^\circ, \pm 90^\circ\}$, as shown in Fig. 3(b).

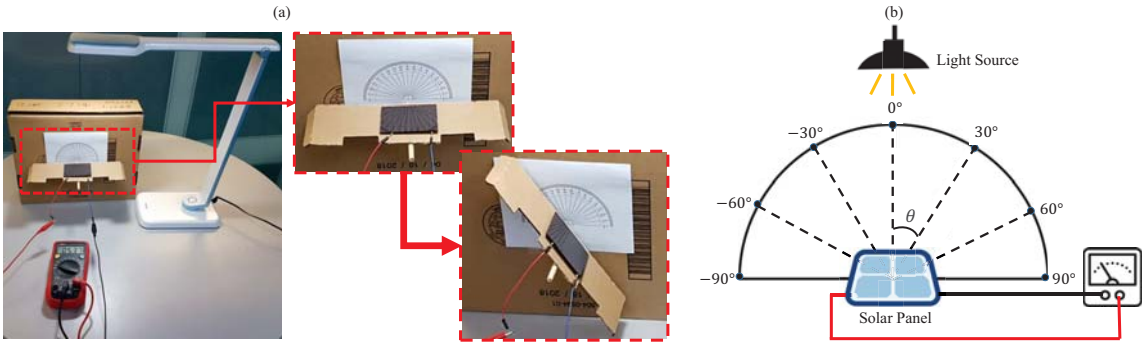

Fig. 3: The measurement setup consists of a solar panel mounted on a handler. (a) the handler allows us to rotate the solar panel to the desired angle; (b) the schematic diagram of the measurement setup.

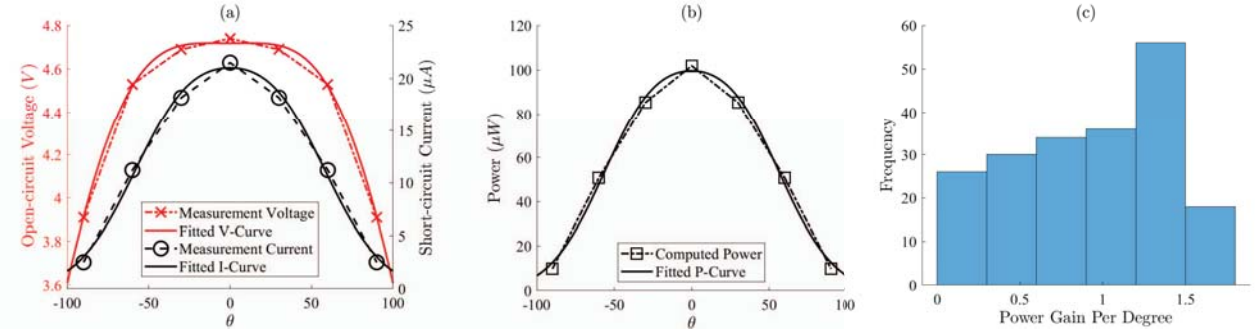

Fig. 4: The relationship between θ and (a) measurement voltage and current, and (b) computed power. (c) The power gain for every 1° increment. Note that the light intensity is fixed at $100lx$.

C. The Implications of the Orientation of the Solar Panel

Let α be the angle between the irradiance beam and the solar panel surface, and θ be the incident angle. Then, we have $\theta = 90^\circ - \alpha$. The relationship between V_{oc} and I_{sc} and the corresponding angle are shown in Fig. 4(a). The dotted line with marker indicates the measurement data we collected by adjusting the solar panel to the corresponding angle. By using the curve fitting tool, the voltage and current curve can be described as follows:

$$\begin{aligned} V(\theta) &= \sum_{k=1}^{2} A_{Vk} \exp(-((\theta - B_{Vk})/C_{Vk})^2) \\ I(\theta) &= \sum_{k=1}^{2} A_{Ik} \exp(-((\theta - B_{Ik})/C_{Ik})^2) \end{aligned} \tag{2}$$

where A_{Vk}, B_{Vk}, and C_{Vk} are the fitted coefficients for the voltage curve, and A_{Ik}, B_{Ik}, and C_{Ik} are for the current curve.

The power can be computed by multiplying V_{oc} and I_{sc}. The resultant power is plotted in Fig. 4(b). Similarly, the power curve is obtained by the same curve fitting tool. The fitted power curve has the same equation format as the voltage and current curve, and the fitted coefficients obtained by the power curve are either the multiplication or the addition of the fitted coefficients obtained for the voltage and current curve. Specifically, the fitted coefficients for the power curve can be described as follows:

$$\begin{aligned} A_{Pk} &= A_{Vk} A_{Ik} \\ B_{Pk} &= B_{Vk} + B_{Ik}, \quad \forall k \in [1,2] \\ C_{Pk} &= -C_{Vk} - C_{Ik}. \end{aligned} \tag{3}$$

In other words, the fitted power curve can be obtained by directly multiplying the voltage and current curve.

From this experiment, it is clear that the power harvested by the solar panel at any instantaneous point of time is dependent on the incident angle. In particular, when we rotate the solar panel such that it is perpendicular to the normal angle, at which $90^\circ - \alpha = 90^\circ - 90^\circ = 0$, the power increases from $85.36\mu W$ to $101.91\mu W$. From our fitted curve, we computed the power gain for every degree, and plotted the histogram, as illustrated in Fig. 4(c). From the histogram, we can see that at least $0.5\mu W$ power gain is obtained for every increment. Furthermore, the maximum power gain happens at the angle between 70° and 20°. Such a power gain tells us that the performance of the solar panel at the same location can be further optimized by adjusting its orientation. Fig. 5 shows a) the power and b) charging time caused by different light intensities with various incident angles, θ on the solar panel surface. Such an insight provides us inspiration for our deployment formulation, presented in Section III.

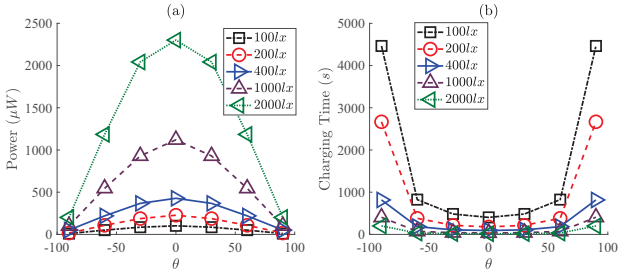

Fig. 5: The orientation of the solar panel θ to the light source at different light intensities has different effects on the (a) generated power and (b) charging time.

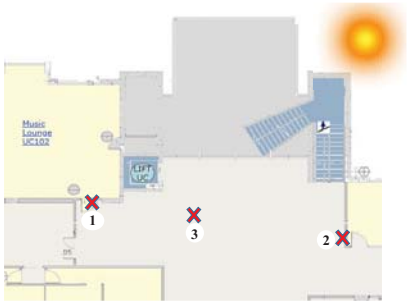

Fig. 6: Three locations indicated with the "x" markers at around noon time are selected to be the deployment location.

III. Beacon Deployment Problem

As discussed, the dimensions of the solar panels used by BLE beacons are relatively small compared to the solar panels installed outside. While a lot of research efforts have been put forward to optimize the performance of solar panels via solar tracking algorithms [16], [17], most works focus on outdoor environments and do not consider the absence of sunlight in indoor environments and at night. The beacon deployment problem can be categorized into two phases: 1) *the initial phase* identifies the deployment location according to the ambient data. 2) *the operational phase* adjusts the angle and the distance of the deployed beacon within the bounded angle and distance to minimize the charging time of the beacon during each operation hour. In this section, we present the beacon deployment problem in indoor environments for both phases.

A. Initial Deployment Phase

Our beacon deployment problem consists of two parts: 1) first, we use a real-world dataset to identify the initial deployment location; 2) second, we use our empirical model (cf. Section II-C) and irradiance model (cf. Section II-A) to simulate the MDP problem.

For the first part, we collected data from a lobby area in a building facing east. Fig. 6 shows the diagram of the lobby. We manually collected the data at many different locations around the lobby. We used a smartphone equipped with light sensor to collect the data, hence the data provides us the light intensity information. Based on the data, we identify three locations for further experiment.

In general, these three locations were selected based on our deployment principles as follows:

1) ***Location 1****:* The first location is directly under one indoor light source. The light intensity recorded at this location is approximately $460lx$. According to the building management, the light source is on for at least 13 hours per day, from $9am$ to $10pm$. This location is selected for further simulation such that we can verify the operation of solar-powered beacon in a scenario when only a single indoor light source is available.

2) ***Location 2****:* The second location is directly under the combination of two light sources. Furthermore, this location might also receive sunlight at a certain time of day, typically when the sun rises. The operation hours of the two light sources are from $9am$ to $10pm$. This location is selected for further simulation because the light intensity at this particular location might vary from our recorded value of 550lx from time to time subject to the sunlight and shadows induced by moving bodies.

3) ***Location 3****:* As shown in Fig. 6, the third location is directly under the sun. The building uses a transparent ceiling in the center of the lobby hall. Hence, the sun light can directly pass through the ceiling glass and incident on our third deployment location. In this case, our third location will get the maximum light intensity around noon when the sun is directly over head. This location is selected to verify the effect of outdoor light sources.

B. Operational Phase: Markov Decision Process (MDP)

The beacon deployment problem is modeled as a discrete-time MDP — a stochastic process that makes decisions to maximize the reward function. The MDP defines a 5-tuple $< S, A, R, T, \gamma >$, where S is a finite set of states, A is a set of actions, R is the reward function, $T(s', a, s)$ is the transition probability from current state s to next state s' given the action a, and $\gamma = [0, 1)$ is the discount factor to regulate the immediate and future reward. We define a 2-tuple state $< C, B >$, where C is a set of deployment location and B is a set of inclination angles. Specifically, $c_s = (x, y, z), \forall c_s \in C$ denotes the deployment location defined according to the 3-dimensional coordinates (x, y, z); and $\beta_s \in B$ is the inclination angle of the solar panel with respect to the horizontal space, as illustrated in Fig. 2. Hence, the total number of states is $|S| = |C| \times |B|$.

The action space defines a set of actions for adjusting the inclination angle of the solar panel with respect to the north-south or east-west orientation. Let A be a set of possible actions to orient the solar panel, then $A = \{East(\beta), West(\beta), North(\beta), South(\beta)\}$. Note that the orientation of the solar panel is based on the desired inclination angle β. The transition probability $T(s', a, s)$ can also be

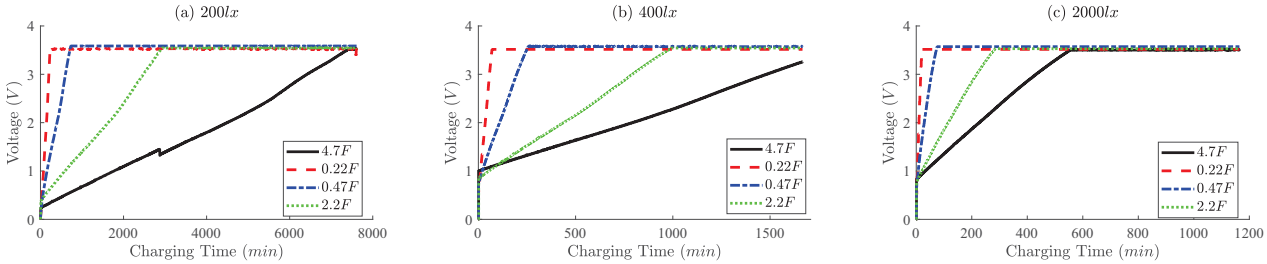

Fig. 7: The charging time for different supercapacitors when the light intensity is equal to (a) 200lx, (b) 400lx, and (c) 2000lx.

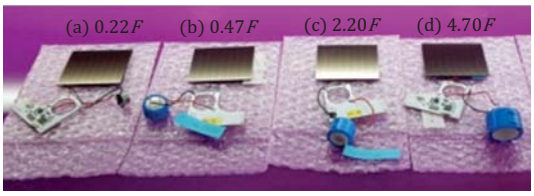

Fig. 8: BLE beacons chipsets with supercapacitors of different values

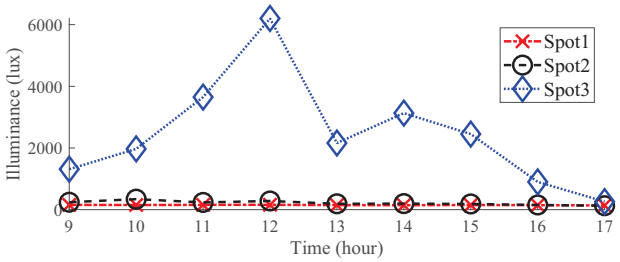

Fig. 9: Light intensity at three locations from 9 am - 5 pm in the lobby hall.

expressed as $P(s'|s,a)$. It defines that the transition to the next state s' is conditioned on the current state $s =< c_s, \beta_s >$ action a. We assume a uniformly distributed transition probability for all possible actions to switch from the current state to the next state. The reward function $R_a(s,s')$ indicates the potential reward to be received when we take an action a to adjust the beacon from the current state s to the next state s'. In this paper, the reward function is defined based on the power gain as described in Section II-C.

The objective of the MDP is to search for a policy $\chi : S \rightarrow A$ that maximizes the long-term reward. In general, the objective function can be defined using the Bellman Equation [18] as follows:

$$V^*(s,a) = \max_a \left(R(s,a) + \gamma \sum_{s' \in S} T(s',a,s) V^*(s') \right) \quad (4)$$

where $V^*(s,a) : S \times A \rightarrow \mathbb{R}$ is the action-value function, and $V^*(s) : S \rightarrow \mathbb{R}$ denotes the value function.

IV. Experiments and Results

This section presents charging time experiments and results to understand the performance of solar-powered beacons with supercapacitors under different light intensity followed by the comparison of power harvested from solar panels of our adjustable solar-powered beacon, luXbeacon and a commercial beacon (i.e., GCell solar beacon). Then, we simulate the angle adjusting problem formulated according to MDP framework with two algorithms, i.e., policy iteration (PI) and value iteration (VI).

A. Charging Time with Different Supercapacitors

As shown in Fig. 8, four BLE beacons with the same solar panel size but different supercapactors (0.22F5.5V, 0.47F5.5V, 2.2F5.5V and 4.7F5.5V) were used to test the charging time under different light intensities. The experiment began by discharging all the supercapacitors to 0V. We used a multimeter to measure the voltage from the supercapacitors. The time to charge the supercapacitors to $3.55-3.6V$ was logged, and the results are plotted in Fig. 7 (a)–(c) given light intensity equal to (a) 200lx, (b) 400lx, and (c) 2000lx. The charging time of the supercapacitor increases when the solar panel is directly under the light source with higher light intensity, as shown in Fig. 7(c) in comparison to (a) and (b). It is clear that the charging time of the supercapacitor follows the conventional RC model.

B. Adjustable Solar Panel vs. Non-adjustable Solar Panel

During the initial deployment phase, three locations were selected to deploy the beacon. We examine these three locations with two type of beacons: 1) a beacon with an adjustable solar panel and 2) a beacon with a non-adjustable solar panel (we used two existing solar-powered beacons in the market, i.e., luXbeacon and GCell beacon). Note that our adjustable solar-powered beacon and luXbeacon have the same size of solar panels and GCell solar panel size is around half of our adjustable beacon and luXbeacon. We also measure the light intensity at these 3 deployment location from 9am to 5pm, as shown in Fig. 9. Fig. 10 illustrates the power of the deployed beacons at these three locations. From Fig. 10, our adjustable solar-powered beacon outperforms luXbeacon and GCell indoor solar-powered beacon in terms of power produced by the solar panel in all three indoor locations in a partly cloudy day because our adjustable solar-powered beacon can react to changing of light environment.

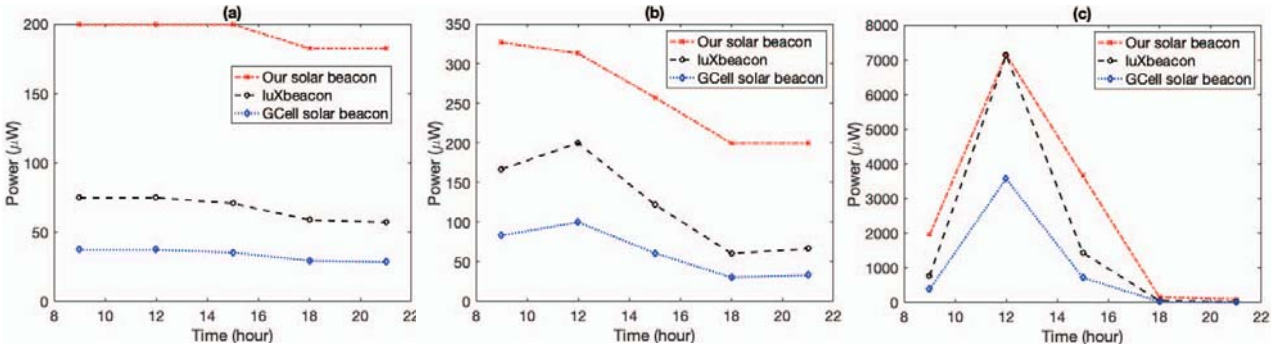

Fig. 10: Power comparison between our adjustable solar-powered beacon, luXbeacon and GCell beacon at (a) location 1, (b) location 2, and (c) location 3 from 9 am to 9 pm in a partly cloudy day.

C. Numerical Simulation

During the simulation, the charging time achieved at every time interval (per hour) was computed and used as the evaluation metric to benchmark the PI in comparison to the VI. We ran a 24-hour simulation by varying the light intensity in the three locations according to the irradiance model described in Section II-A. The simulation results indicate that the VI and PI can make good decisions to achieve similar fast charging times in all three deployment spots. Overall, both VI and PI achieve equally rapid charging efficiency, making frequent decisions to adjust the angle when necessary.

V. Conclusion

Solar-powered beacons present a more challenging deployment problem compared to battery-powered beacons. In this paper, we employ the MDP to formulate the deployment problem and to search for the optimal decision at every hourly interval. The major contribution of this work is integrating the power gain into the MDP's reward function. Based on our reward function, we solve the MDP problem using VI and PI methods to make the decision for the best action to take at every hourly interval. The results indicate that the PI and VI algorithms can make reasonably good decisions for fast charging time. In addition, our adjustable solar-powered beacon harvested more energy significantly than conventional solar-powered beacons when light environment changes. Such high power produced from the solar panel and fast charging time is essential to ensure that a beacon can still maintain its operation during odd hour when both indoor and outdoor light sources are not available.

Acknowledgment

This work was supported by HKUST-NIE Social Media Laboratory.

References

[1] K. E. Jeon, J. She, P. Soonsawad, and P. C. Ng, "Ble beacons for internet of things applications: Survey, challenges, and opportunities," *IEEE Internet of Things Journal*, vol. 5, no. 2, pp. 811–828, April 2018.

[2] D. Hortelano, T. Olivares, M. C. Ruiz, C. Garrido-Hidalgo, and V. López, "From sensor networks to internet of things. bluetooth low energy, a standard for this evolution," *Sensors*, vol. 17, no. 2, p. 372, 2017.

[3] M. Papandrea, S. Giordano, S. Vanini, and P. Cremonese, "Proximity marketing solution tailored to user needs," in *World of Wireless Mobile and Multimedia Networks (WoWMoM), 2010 IEEE International Symposium on a*. IEEE, 2010, pp. 1–3.

[4] P. C. Ng, J. She, and S. Park, "Notify-and-interact: A beacon-smartphone interaction for user engagement in galleries," in *2017 IEEE International Conference on Multimedia and Expo (ICME)*, July 2017, pp. 1069–1074.

[5] R. Faragher and R. Harle, "Location fingerprinting with bluetooth low energy beacons," *IEEE Journal on Selected Areas in Communications*, vol. 33, no. 11, pp. 2418–2428, Nov 2015.

[6] C. H. Lam, P. C. Ng, and J. She, "Improved distance estimation with ble beacon using kalman filter and svm," in *2018 IEEE International Conference on Communications (ICC)*, May 2018, pp. 1–6.

[7] P. C. Ng, J. She, and R. Ran, "A compressive sensing approach to detect the proximity between smartphones and ble beacons," *IEEE Internet of Things Journal*, pp. 1–1, 2019.

[8] K. E. Jeon, J. She, J. Xue, S. Kim, and S. Park, "luxbeacon -a batteryless beacon for green iot: Design, modeling, and field tests," *IEEE Internet of Things Journal*, pp. 1–1, 2019.

[9] N. Dang, R. Valentini, E. Bozorgzadeh, M. Levorato, and N. Venkatasubramanian, "A unified stochastic model for energy management in solar-powered embedded systems," in *Proceedings of the IEEE/ACM International Conference on Computer-Aided Design*. IEEE Press, 2015, pp. 621–626.

[10] A. A. Panagopoulos, G. Chalkiadakis, and R. N. Jennings, "Towards optimal solar tracking: a dynamic programming approach," 2015.

[11] F. Kreith and J. F. Kreider, "Principles of solar engineering," *Washington, DC, Hemisphere Publishing Corp., 1978. 790 p.*, 1978.

[12] N. Piovesan and P. Dini, "Unsupervised learning of representations from solar energy data," in *2018 IEEE 29th Annual International Symposium on Personal, Indoor and Mobile Radio Communications (PIMRC)*, Sep. 2018, pp. 1–6.

[13] G. A. Kamali, I. Moradi, and A. Khalili, "Estimating solar radiation on tilted surfaces with various orientations: a study case in karaj (iran)," *Theoretical and applied climatology*, vol. 84, no. 4, pp. 235–241, 2006.

[14] B. Liu and R. Jordan, "Daily insolation on surfaces tilted towards equator," *ASHRAE J.;(United States)*, vol. 10, 1961.

[15] A. Luque and S. Hegedus, *Handbook of photovoltaic science and engineering*. John Wiley & Sons, 2011.

[16] J. Rizk and Y. Chaiko, "Solar tracking system: more efficient use of solar panels," *World Academy of Science, Engineering and Technology*, vol. 41, pp. 313–315, 2008.

[17] S. Yilmaz, H. R. Ozcalik, O. Dogmus, F. Dincer, O. Akgol, and M. Karaaslan, "Design of two axes sun tracking controller with analytically solar radiation calculations," *Renewable and Sustainable Energy Reviews*, vol. 43, pp. 997–1005, 2015.

[18] R. Bellman, "The theory of dynamic programming," RAND Corp Santa Monica CA, Tech. Rep., 1954.